Resonance Ultrasound Spectroscopy Forward Modeling and Inverse Characterization of Nickel-based Superalloys

Eric Biedermann[2, a)], Leanne Jauriqui[2, b)], John C. Aldrin[3,c)], Brent Goodlet[4,d)], Tresa Pollock[4,e)], Chris Torbet[4,f)], Siamack Mazdiyasni[1,g)]

[1]Air Force Research Laboratory (AFRL/RXCA), Wright-Patterson AFB, OH 45433, USA
[2]Vibrant Corporation, Albuquerque, NM 87113, USA
[3]Computational Tools, Gurnee, IL 60031, USA
[4]University of California, Santa Barbara, Santa Barbara, CA 93106, USA

[a)]Eric Biedermann: ebiedermann@vibrantndt.com
[b)]Leanne Jauriqui: ljauriqui@vibrantndt.com
[c)]John Aldrin: aldrin@computationaltools.com
[d)]Brent Goodlet: bgoodlet@engineering.ucsb.edu
[e)]Tresa Pollock: pollock@engineering.ucsb.edu
[f)]Chris Torbet: ctorbet@engineering.ucsb.edu
[g)]Siamack Mazdiyasni: siamack.mazdiyasni@us.af.mil

Abstract. The objective of this paper is to investigate Resonance Ultrasound Spectroscopy (RUS) measurement models to more precisely connect changes in the resonance frequencies of nickel-based super-alloy material to the macro/microscopic state. RUS models using analytical solutions and the finite element method (FEM) were developed to address varying elastic properties, grain structures and creep. Experimental studies were performed investigating the effect of exposure to high temperatures and stress for varying part shape and three grain structure classes: single crystals, directionally-solidified and polycrystalline structures. Inversion using both traditional analytical models was enhanced in order to simultaneously estimate varying material properties and changes in part geometry due to creep. Inversion using surrogate models from FEM simulations was also developed, addressing varying crystal orientation and complex geometries. Results are presented comparing the forward model trends and inversion results with nickel alloy parts under various test conditions.

INTRODUCTION

Resonance Ultrasound Spectroscopy (RUS) is a method for non-destructive evaluation (NDE) and material characterization that uses the ultrasonic resonance frequencies of a component [1]. Vibrant Corporation combines RUS with advanced pattern recognition algorithms and statistical scoring to field Process Compensated Resonance Testing (PCRT) for commercial NDE applications [2]. Among the most critical of those applications are gas turbine engine blades made from nickel-based superalloys [3]. Figure 1 shows a turbine blade from the JT8D turbofan engine on a PCRT test fixture. In testing of turbine blades, Vibrant has demonstrated sensitivity of resonance frequencies to material conditions like overtemperature exposure that reduces creep resistance in the Ni-base superalloy material. Figure 2(a) shows the sensitivity of resonance frequencies to increasing exposure temperatures. By applying statistical scoring to resonance frequencies identified as diagnostic by its pattern recognition algorithms, Vibrant's PCRT sorting module inspects every blade in an engine set for exposure to unacceptable temperatures. PCRT earned FAA approval [4] to be used instead of a destructive cutup sampling of one blade from a suspect engine set.

41st Annual Review of Progress in Quantitative Nondestructive Evaluation
AIP Conf. Proc. 1650, 835-844 (2015); doi: 10.1063/1.4914687

Historically, RUS-based inspections require the collection of a large quantity of empirical data in the form of resonance frequencies and part classifications to serve as a training set. Going forward, there is a critical need for quantitative models to more precisely relate changes in the material state, ideally from the micro and the macro-scales, with the resonance behavior of the material. As turbine engines age and lose exhaust gas temperature margin, the combined temperature and stress on the airfoils eventually cause the airfoil microstructure to undergo gradual changes resulting in a reduction of strength and creep resistance. Prior work on gas turbine airfoils exposed to high temperature and stress has shown that RUS is capable of measuring consistent correlated shifts in resonance frequency peaks [3-4]. However, it should be recognized that in real engineered structures, such as gas turbine engines, multiple damage mechanisms often occur simultaneously, confounding the interpretation of the shift in frequency peaks.

The objective of this effort is to develop and enhance RUS measurement models to more precisely connect changes in the resonance frequencies of nickel-based superalloy material subject to the macro/microscopic state. This work builds on past work inverting RUS data for elastic property characterization of parts with canonical shapes [1,5] and recent RUS modeling for damage characterization of silicon nitride balls [6]. RUS models using both enhanced analytical models and finite element method were developed demonstrating the ability to simulate varying elastic properties, geometry, crystal orientation, grain structures and creep. A comprehensive test plan was also conducted, investigating the effect of exposure to high temperatures and stress for varying part shape and three grain structure classes: single crystals (SX), directionally-solidified structures (DS) and polycrystalline structures (PX). To address more sophisticated material and geometric conditions, new RUS property inversion tools were developed. Inversion using traditional analytical models was enhanced in order to simultaneously estimate varying material properties and possible changes in part geometry, for example due to creep. As well, the capability of performing inversion using surrogate models from FEM data was developed, providing greater flexibility to evaluate varying crystal orientation and address complex geometries. Results are presented comparing the forward model trends and inversion results with nickel alloy parts under various test conditions.

FIGURE 1. JT8D turbine blade on PCRT test fixture.

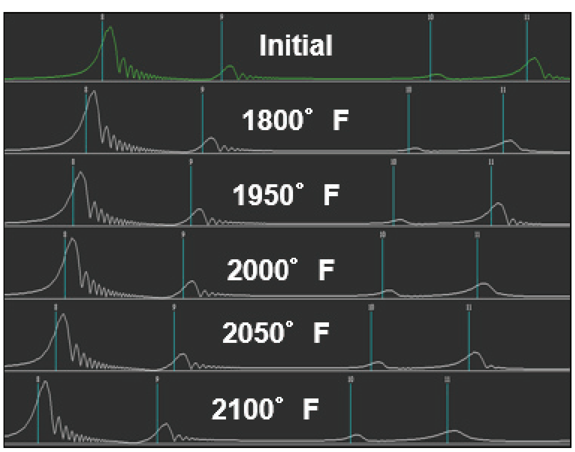

(a)

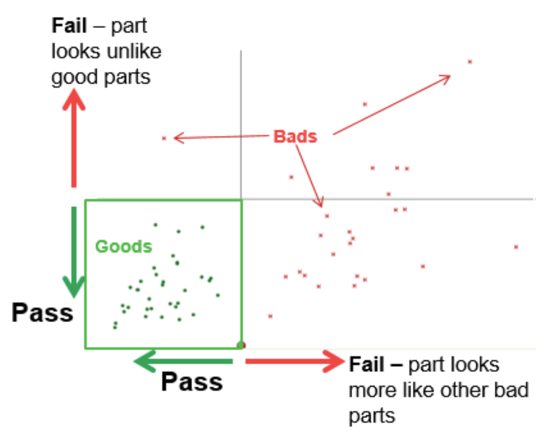

(b)

FIGURE 2. Vibrant experience with RUS for Ni-base superalloy, (a) frequency sensitivity to overtemperature exposure, (b) PCRT PASS/FAIL scoring plot for production sorting module.

TEST SPECIMENS

To study and model the effect of material variation, temperature exposure and stress conditions on propulsion system components on RUS, the nickel-based superalloy Mar-M247 was selected for this project. While older than many turbine blade materials used today, a great deal of experience with Mar-M247 exists in production NDE and material research. As well, because it has been extensively characterized and is relatively affordable, Mar-M247 was an attractive choice. As-cast samples of PX, DS and SX Mar-M247 were procured for the experimental studies as shown in Figure 3(a). The as-cast samples were machined into two precise geometries: 1) 3.0" length x 0.5" diameter right cylinders for over-temperature and other material experiments shown in Figure 3(b), and 2) dog bone samples for creep and fatigue experiments shown in Figure 3(c).

(a) (b) (c)

FIGURE 3. (a) As-cast Mar-M247 samples. PX (top), DS (middle), SX (bottom). (b) 3.0" x 0.5" cylinder in test fixture, (c) dog bone samples for creep and fatigue experiments.

RUS FORWARD AND INVERSE MODELING

Much prior work [3-4] has addressed models for RUS and PCRT testing for a variety of object shapes and materials using analytical models and finite element method (FEM) simulation. However, such models often incorporate simplifications and approximations in terms of part geometry, material properties and test conditions that can limit their use for quantitative studies and model-based inversion. Comprehensive RUS forward models are needed which address all key characteristics of the nickel-alloy test specimens and RUS testing conditions that influence the RUS resonance frequencies and mode shapes (Fig. 4). Key testing and specimen characteristics include the following:

- Test Specimen Part Geometry: Part shape and dimensions, macro-scale grain structure (e.g. SX, DS, EQ), coating dimensions, strain due to creep, and dimension changes due to changes in residual stress.
- Macro-scale Material Properties: Elastic properties (E, ν, $\mathbf{C}_{xx}$), 'effective' elastic properties (approximate models of complex grain structures), macro-scale grain orientation, density, coating material properties, and localized (macro-scale) damage (local changes in elastic properties).
- Internal Stress State: Residual stress, profile with depth.
- RUS Test Conditions: Transducer performance (source, receiver), Transducer location, part orientation in fixture, temperature conditions, data sampling rate, and shot-to-shot variation.

Another key objective of this program is to better link, through *material state models,* the material microstructure and thermal and stress state over time to the macro-scale properties of the test specimen and resonance behavior. Potential material state model factors include:

- Material Micro-structure: Matrix material properties, precipitates properties, volume fraction, lattice changes (coarsening, coherence).
- Material State Models: Casting, solutioning, & aging models (standard process), thermal exposure models, creep models, rafting (direct. coarsening) models, fatigue models.

RUS models using analytical and FEM approaches were developed and extended to represent the identified key factors including varying elastic properties, geometry (creep), crystal orientation, grain structure and creep. For this program, two implementations of the analytical model were used: the RUSpec program co-developed with Albert Migliori [1,5] and distributed by Magnaflux Quasar Systems, and a MATLAB implementation originally developed by Matt Fig [7-8]. The RUSpec program models various crystalline material geometries, ranging from isotropic (2 degrees of freedom) to orthorhombic (9 degrees of freedom). Material properties are defined in terms of the elastic tensors, C_{xy}, of elastic constant matrix that relate the stress and strain tensors in the theory of elasticity [9]:

$$\begin{pmatrix} \sigma_1 \\ \sigma_2 \\ \sigma_3 \\ \sigma_4 \\ \sigma_5 \\ \sigma_6 \end{pmatrix} = \begin{pmatrix} C_{11} & C_{12} & C_{13} & C_{14} & C_{15} & C_{16} \\ C_{21} & C_{22} & C_{23} & C_{24} & C_{25} & C_{26} \\ C_{31} & C_{32} & C_{33} & C_{34} & C_{35} & C_{36} \\ C_{41} & C_{42} & C_{43} & C_{44} & C_{45} & C_{46} \\ C_{51} & C_{52} & C_{53} & C_{54} & C_{55} & C_{56} \\ C_{61} & C_{62} & C_{63} & C_{64} & C_{65} & C_{66} \end{pmatrix} \begin{pmatrix} \varepsilon_1 \\ \varepsilon_2 \\ \varepsilon_3 \\ \varepsilon_4 \\ \varepsilon_5 \\ \varepsilon_6 \end{pmatrix}. \tag{1}$$

Cubic material models were first considered to address SX Mar-M247 and approximate DS Mar-M247 where the elastic matrix can be expressed in terms of only three independent parameters, C_{11}, C_{12}, and C_{44}. For PX Mar-M247, an approximate isotropic material model was first considered where:

$$E = \frac{C_{44}(3C_{11} - 4C_{44})}{(C_{11} - C_{44})}, \tag{2}$$

$$\nu = \frac{(C_{11} - 2C_{44})}{2(C_{11} - C_{44})}. \tag{3}$$

However, these analytical models could not be modified to address arbitrary crystalline material orientation and complex part geometry such as for the dog-bone specimen. Three FEM software packages, Abaqus, ANSYS and COMSOL, were used by the team, with good agreement for verification test problems.

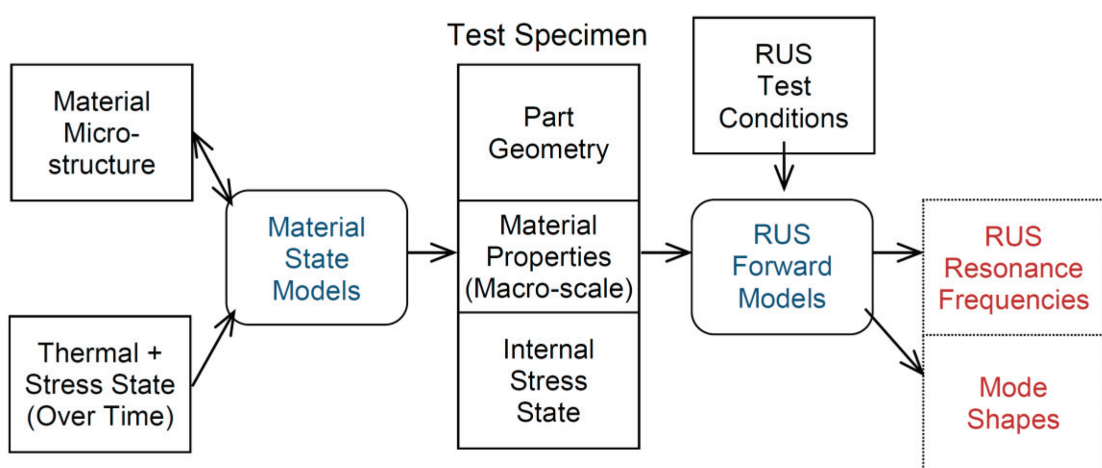

FIGURE 4. RUS forward model schematic.

Convergence and error studies were performed to verify the accuracy of the models. Figure 5 shows the percent difference in the resonance frequencies for a 3.0" x 0.5" PX Mar-M247 cylinder between the FEM model at the highest mesh resolution (for the desktop PC) and analytical results with varying polynomial model order corresponding with numerical accuracy. Certain low order modes were found to converge quickly to the finely meshed FEM results. The RUSpec analytical model software was constrained to a maximum polynomial order of 14 which was found to exhibit some solution error around mode 20 and significant error beyond mode 30. Because of the long, thin aspect ratio of the test cylinder, a very high polynomial order was necessary to precisely represent many of the complex mode shapes beyond mode 30. A polynomial order of 22 produced a very good match with FEM results through mode 80. Note, this trend would be less severe for a part with more similar dimensions in the x, y, and z-directions. This model error evaluation is critical since only simulated results using a validated model should be used for RUS quantitative studies and inverse characterization.

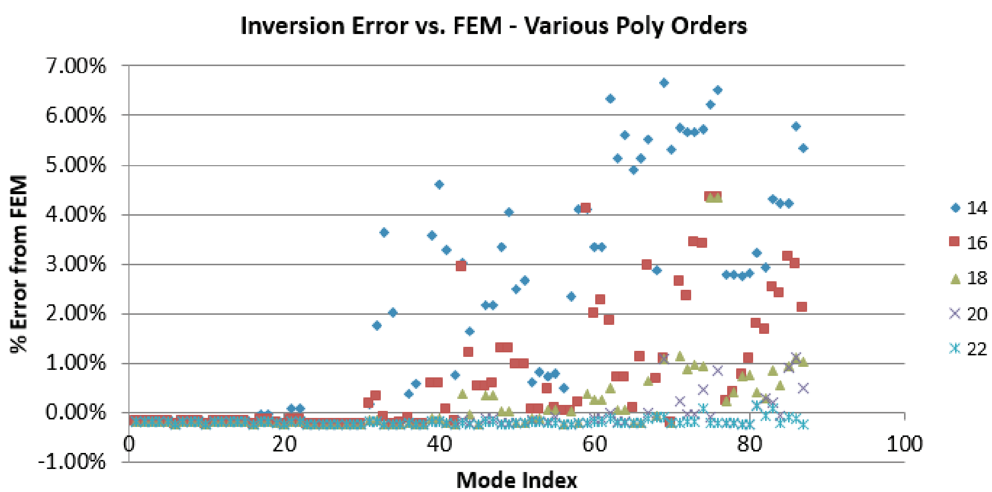

FIGURE 5. Inversion error between FEM and analytical models for varying analytical model polynomial order.

The vision for this effort, shown in Fig. 6, is to develop model-based inverse methods that precisely connect measured changes in the resonance frequencies of parts under test to a quantitative evaluation of the macro-scale test specimen, micro-structure material state and ideally, life prediction. RUS property inversion tools were developed in Matlab to provide some of this quantitative inversion capability. The conventional RUS inversion algorithms were enhanced with the addition of parameters to simulate asymmetry in material properties and changes in geometry due to creep and other loads. As well, the capability of performing inversion using surrogate models from FEM data was developed, providing greater flexibility to evaluate varying crystal orientation and address complex geometries.

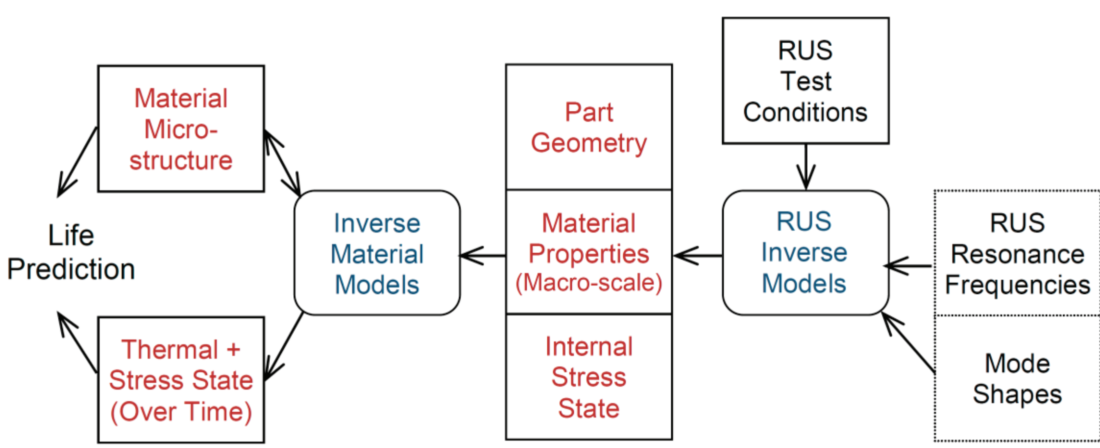

FIGURE 6. RUS inverse model schematic.

RESULTS

Parametric studies were performed to examine the effect of the modeling variables on the resulting resonance frequencies. Both the geometric and material properties of a sample coupon were varied to gauge the resulting change in resonance frequencies. The analytical model was used to generate the first 100 mode frequencies for a baseline cylinder, with properties designed to represent Mar-M247: diameter = 1.27 cm, length = 7.62 cm; density = 8.57 g/cm^3, C_{11} = 315 GPa, C_{44} = 83 GPa, E = 219.3 GPa, and ν = 0.321. Models were also generated by varying the diameter, length and/or density of the sample, +/- 1.0%, one factor at a time (OFAT). When the length or diameter was changed, the density was retained, such that the modeled sample weight also changed. Figure 7 shows the resonance frequency changes, by mode index associated with increasing resonance frequencies, for the first 25 modes of the sample cylinder, for the changes to length, diameter and density. The plot here is symmetrical with only the positive frequency shifts shown. Mode images from ANSYS are presented in Figure 7(b) through Figure 7(d) for bending, breathing and torsion modes respectively. Density and Young's modulus (E) changed all modal frequencies uniformly on a percent change basis. Diameter and C_{11} changed bending and breathing modes, but did not affect torsional modes at all. Length changed all frequencies, but bending and breathing modes were more sensitive. C_{44} changed torsional modes more than breathing or bending. As well, Poisson's ratio (ν) had an effect on the torsional modes with very little effect on breathing or bending only at high frequencies. Thus by using these observed unique changes in properties for the three main mode types, it is possible to evaluate associated changes in global elastic properties for a limited number of material parameters.

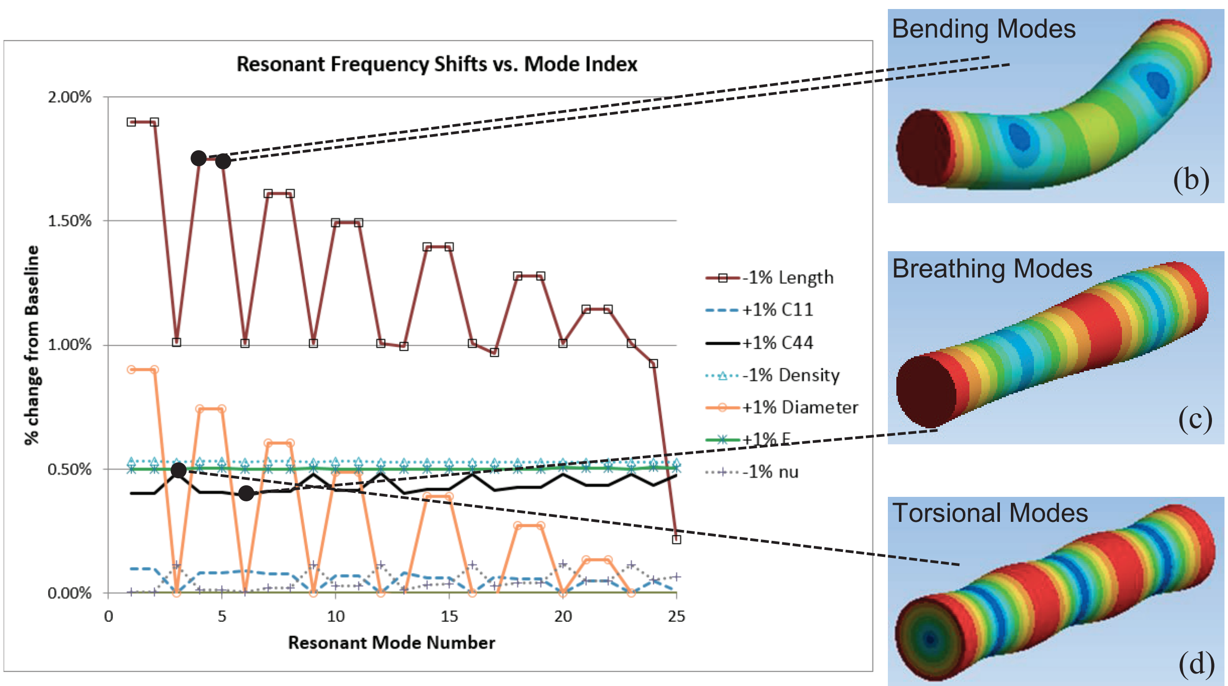

FIGURE 7. (a) Cylinder parameter study results with mode matching for (b) bending, (c) breathing and (d) torsional modes.

A set of PX cylinders were tested using RUS over a series of aging and solutioning heat treatments in a vacuum furnace. Figure 8 shows the heat treatment frequency shift data after (1) a 24 hr period at 1080°C and (2) a subsequent 2 hr solutioning treatment at 1200°C. The modeled data was compared to measured data for PX Mar-M247 samples which had undergone aging heat treatments, to assess which property changes most likely explained the changes measured in the samples. By comparing the trends in Figure 7 with the first heat treatment in Figure 8, it is clear that the aging heat treatment of physical cylinders changed all mode types, but changed the torsional modes more than breathing or bending modes. The trend here is very similar to the C_{44} trend observed in the parameter study plot in Figure 7. Applying a scale factor to the C_{44} trend found that a C_{44} increase of 0.35% closely matched the frequency change caused by the cylinder heat treatments.

A Matlab application was developed specifically to invert frequency *changes*, to determine the most likely material property change due to these aging heat treatments using both analytical and FEM surrogate models. Figure 9 plots inverted estimates of the change in the global material properties, the effective elastic modulus (E) and shear modulus (G), for a series of heat treatments at 870°C. Both values show clear, smooth trends with respect to exposure time at the aging heat treatment temperature. Ideally, one would like to connect this change in the 'effective' material properties for aging heat treatments with material state models. Results from these studies show some sensitivity of changes in global elastic properties to aging heat treatments and solutioning; however, it is difficult to precisely connect these changes to the material microstructure state at this time. More research and material characterization is needed to ideally build such materials state models.

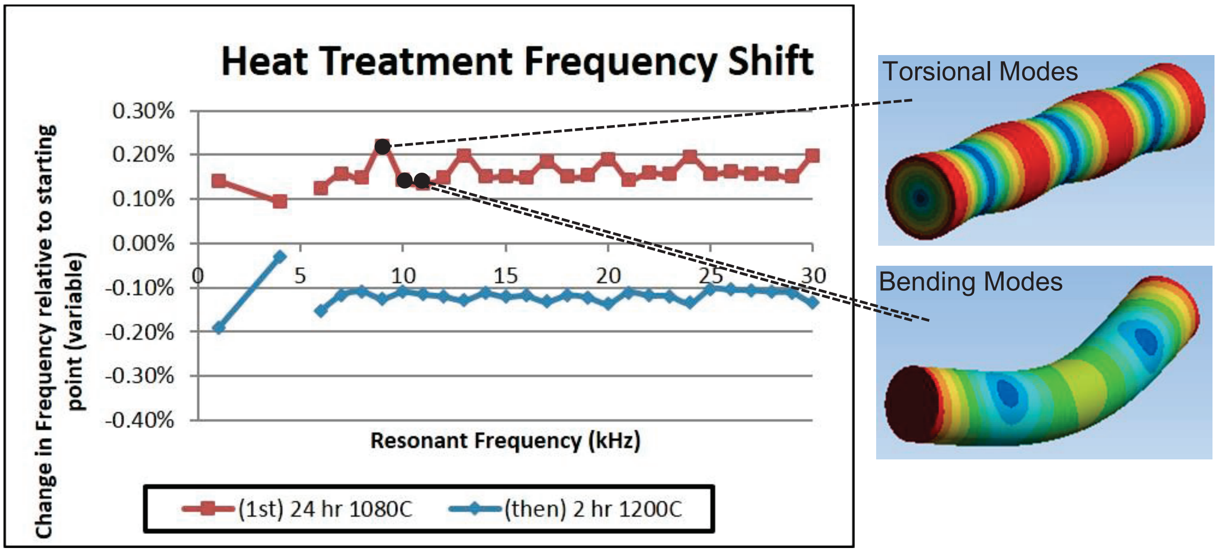

FIGURE 8. Heat treatment frequency shift data with mode matching.

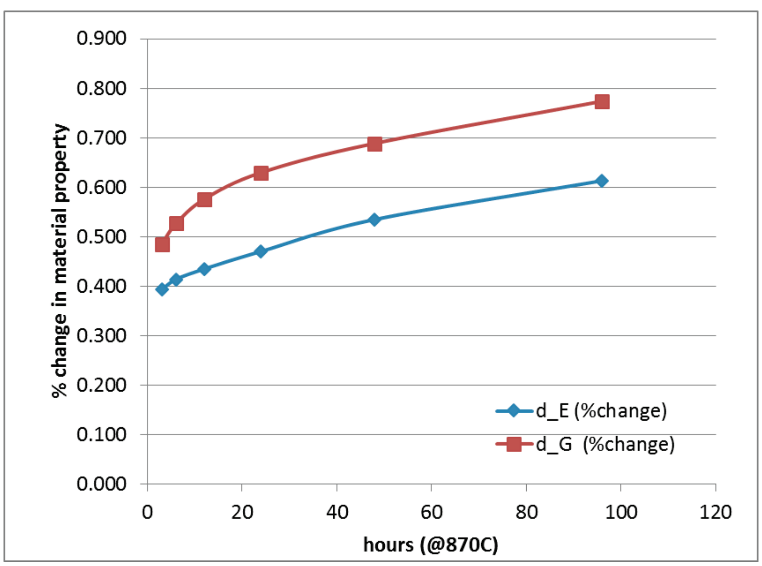

FIGURE 9. Inversion of changes in aggregate elastic properties for a series of aging heat treatments at 870°C.

Model inversions were also used to estimate the absolute elastic properties of each of the three grain structure class samples. The inversion results were found to be in agreement with expectation for both cylindrical and parallelepiped geometries. Due to space limitations, only a summary of key findings from the inversion studies is presented here. For SX specimens, the importance of addressing varying crystal orientation using a finite element generated surrogate model with five unknowns (three cubic material properties and two angles for the crystal orientation) was demonstrated. Monte Carlo simulations were performed for varying DS grain structures using FEM with varying distributions for the crystal orientations. Although it was possible to show sets of crystal orientation conditions that will produce a better fit with the data, it is very hard to be quantitative because of the complexity of the material and grain structure. Isotropic models were found to be generally satisfactory for representing PX specimens and achieved good agreement with results from polycrystalline 'averaging' techniques considering varying gamma and gamma-prime volume fractions. Attempts were made to improve the model fit for PX specimens by considering additional components in the model beyond purely isotropic conditions. First, aligning with Kuhn and Sockel [10], the PX specimens were considered to be weakly anisotropic. Second, an extension to the cubic material model considering differences in C_{44} and C_{55} was found to best address degenerate bending modes observed experimentally as shown in Figure 10(a). By considering a weak deviation from isotropic behavior through including anisotropy and degeneracy terms, a more precise representation of the RUS frequency spectrum from modes 7-24 was achieved, as shown in Figure 10(b).

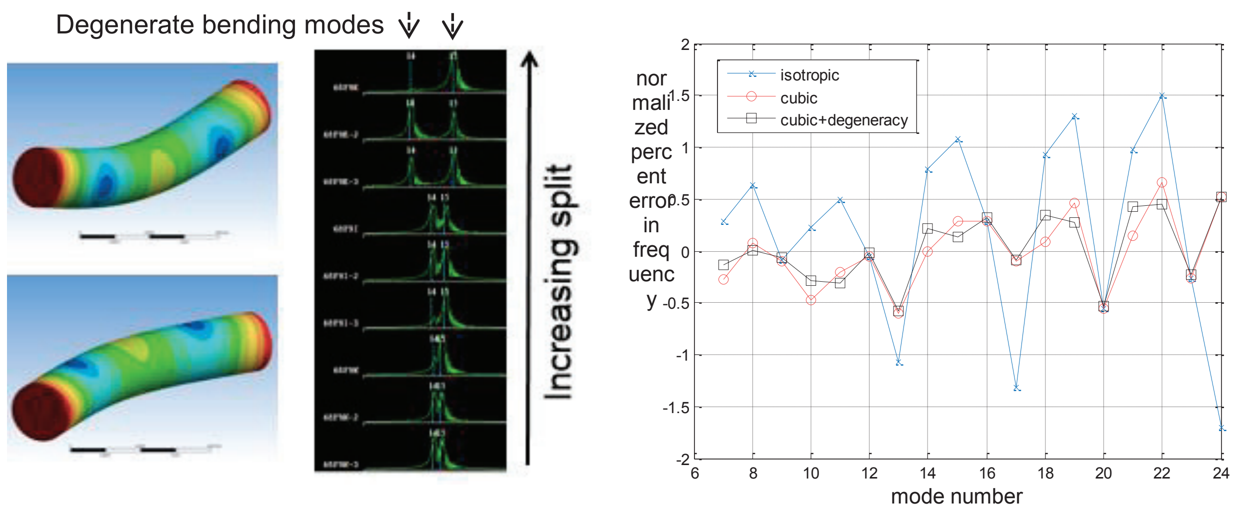

(a) (b)

FIGURE 10. (a) Example of degenerate bending mode shapes and frequency splitting, (b) Comparison of material models for inverse fit error.

To develop a comprehensive model of the changing resonant behavior as a function of creep damage accumulation, simultaneous material and geometric changes must be considered. The complexity of the sample dog-bone shape favors the FEM workspace. The dog-bone model mesh is shown in Figure 3(c) and the isotropic material properties used for the study are as follows: density = 8.55 g/cm^3, E = 215.3 GPa, and ν = 0.313. Modeling the shape change associated with creep was accomplished with a nonlinear plastic analysis, which is generally more straightforward than a full creep plasticity analysis and should yield very similar deformation characteristics. The deformation plasticity model for FEA is represented in one dimension with:

$$E\varepsilon = \sigma + \alpha\sigma\left(\frac{|\sigma|}{\sigma_o}\right)^{n-1}, \tag{4}$$

In Eq. 4, σ is stress, E is Young's modulus, ε represents strain, σ_o is the yield strength, α is a yield offset and n is the hardening exponent typically > 5 for metal plasticity. The three dimensional constitutive law additionally requires a Poisson's ratio, and fully defines the material with nonlinear elastic-plastic properties at all stress levels. However, due to the large exponent n, the elastic response of the material is effectively linear elastic until applied stresses are on the order of the yield strength. When employing a plastic analysis, and applying a finite extension of the sample equivalent to 2 to 20% creep strain, it was necessary to refine the mesh of the gauge section of the dog-bone model to minimize excessive distortion of elements. Using the Abaqus FEM code, the first 50 resonance modes were calculated for samples with varying levels of creep. Figure 11 presents the percentage change from the baseline model on a per-mode basis for varying creep from 2% – 20%.

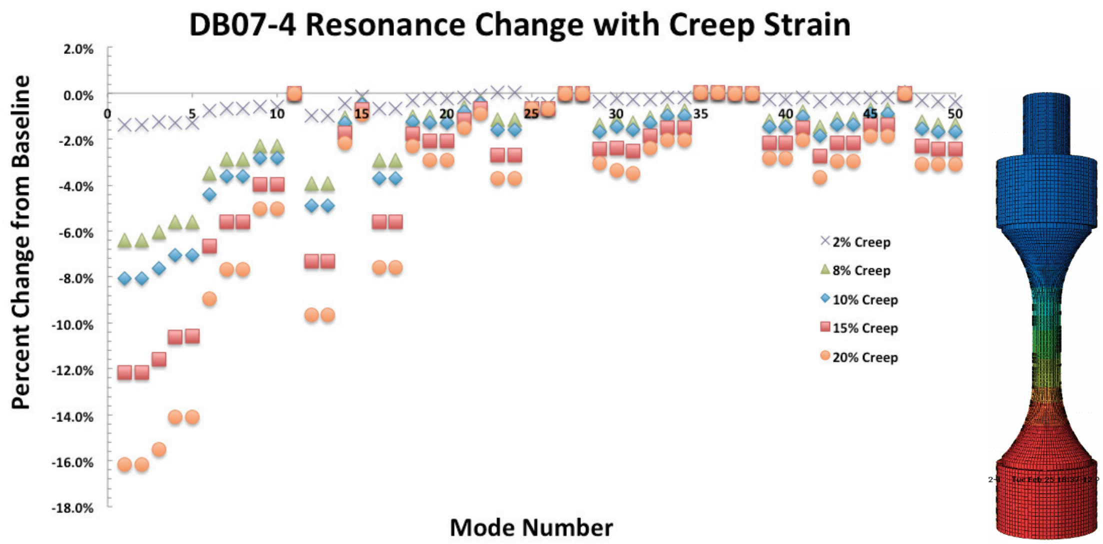

FIGURE 11. Mode-order comparison of first 50 resonance modes plotted against the percent difference from the baseline resonance frequency. The modes are simply compared by their order of occurrence, i.e. lowest to highest frequency.

Iterative creep experiments were conducted at 950°C to mirror operating temperatures commonly experienced by super-alloys in the hot section of a turbine engine. Initial load parameters were aggressive, set at 300 MPa, in an attempt to accelerate the creep experiments and minimize the time-at-temperature. A sample was subjected to six iterations of creep damage and resonance measurements, as well as a pretreatment at 1080°C for 13 hours to further age the γ' microstructure before subjecting the sample to creep. Figure 12 shows this measure-to-model comparison from which we can draw the conclusion that some of the measured change in resonance frequency for this sample is captured through properly accounting for the change in specimen shape. Further analysis is required to determine how the differences that remain between measurements and current models, particularly divergence of peaks deemed insensitive to the shape change associated with creep, can be attributed to other changes in the sample. Other observations of prime interest for further investigation would be degenerate mode pair splitting, and whether this change is associated with random variability and imperfections of the samples, evolution of creep damage, or other parameters of interest to NDE.

CONCLUSIONS AND FUTURE WORK

RUS models using analytical models and the finite element method were developed demonstrating the ability to simulate varying elastic properties, grain structures and creep damage. Experimental studies were performed investigating the effect of exposure to high temperatures and creep on Mar-M-247 Ni-base superalloy with SX, DS and PX grain structures. Forward models for both cylindrical and dog-bone specimens were used to explain the trends in resonance frequency shifts observed in the experimental data. Future work is planned to further resolve the multiple damage mechanisms in propulsion components, ideally addressing heat damage, creep and fatigue, through a model-assisted evaluation approach of the resonance frequencies. A parallel project is underway to quantify uncertainty in RUS models and measurements to maximize the accuracy of forward and inverse RUS models.

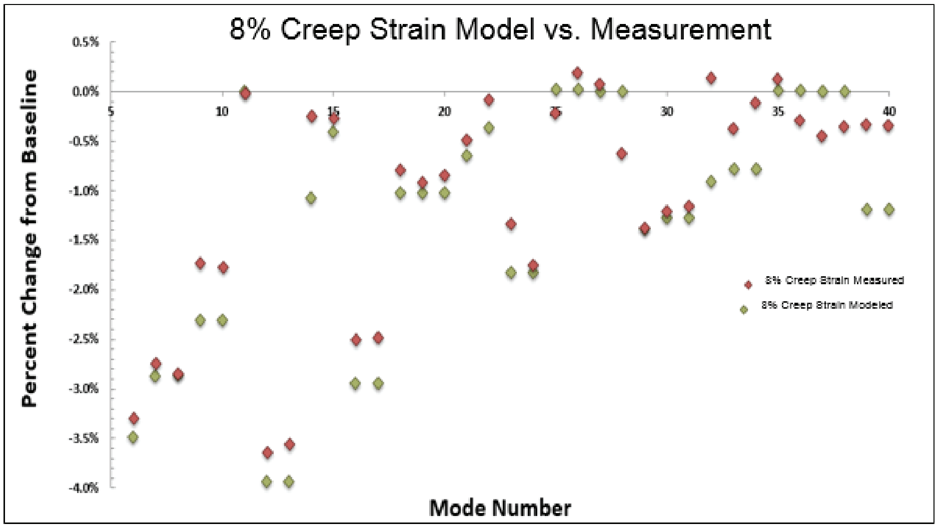

FIGURE 12. Mode-type comparisons of 8% creep strain model and specimen creep experiment to baseline showing that some, but not all, of the measured change in resonance frequency is captured through properly accounting for the change in specimen shape.

ACKNOWLEDGMENTS

This work was supported by the U.S. Air Force Research Laboratory (AFRL) through Research Initiatives for Materials State Sensing (RIMSS) Contract FA8650-10-D-5210, through Universal Technology Corporation. The authors would like to acknowledge the use of Matlab code by Matt Fig for RUS modeling and thank Eric Lindgren for support and feedback on the program. This paper has been cleared for public release by AFRL under case number 88ABW-2014-4562.

REFERENCES

1. Migliori, A., Sarrao, J., Visscher, M. W., Bell, T., Lei, M., Fisk, Z., and Leisure, R., ‘‘Resonant ultrasound spectroscopy techniques for measurement of the elastic moduli of solids,’’ *Physica B*, **183**, 1–24 (1993).
2. Schwarz, J., Saxton, J., and Jauriqui, L., "Process Compensated Resonant Testing in Manufacturing Process Control," *Material Evaluation*, **63** 736-739, (July 2005).
3. Piotrowski, D., Hunter, L., and Sloan, T., "Process Compensated Resonance Testing JT8D-219 1st Stage Blades," ATA NDT Forum 2008, (September 24, 2008). [http://www.vibrantndt.co.uk/files/2008_ATA_NDT_Forum-PCRT_of_JT8D-T1_Blades.pdf].
4. Federal Aviation Administration, Atlanta Aircraft Certification Office (2010). A/W File No.: G2010-07 5087.
5. Migliori, A. and J. L. Sarrao, *Resonant Ultrasound Spectroscopy*, New York, Wiley, (1997).
6. Aldrin, J. C., Jauriqui, L., Hunter, L., "Models for Process Compensated Resonant Testing (PCRT) of Silicon Nitride Balls," *Review of Progress in QNDE*, Vol. 32, AIP, pp.1393-1400, (2013).
7. Fig, M. K., *Resonance Ultrasound Spectroscopy in Complex Sample Geometry*, Master's Thesis, Montana State University, (November 2005).
8. Fig, M. K., "Resonant Ultrasound Spectroscopy (RUS)", Matlab File Exchange, Web Site: http://www.mathworks.com/matlabcentral/fileexchange/11399-resonant-ultrasound-spectroscopy--rus-.
9. Gould, P. L., *Introduction to Linear Elasticity*. New York: Springer, (1994).
10. Kuhn, H-A. and Sockel, H-G, "Elastic Properties of Textured and Directionally Solidified Nickel-based Superalloys Between 25 and 1200° C," *Materials Science and Engineering, A112,* 177-126, (1989).